AIAA JOURNAL
Vol. 40, No. 11, November 2002

Interaction of a Synthetic Jet with a Crossflow Boundary Layer

Douglas R. Smith*
University of Wyoming, Laramie, Wyoming 82071-3295

An experimental investigation of the interaction between a synthetic jet actuator array and a turbulent boundary layer ($Re_\theta = 1.79 \times 10^3$) is reported. The array consisted of three adjacent, parallel synthetic jet actuators, each with a rectangular orifice having an aspect ratio of 45. The effect of the orientation of the jet orifice, relative to the mean freestream direction, on the jet/boundary-layer interaction was investigated. The steady, spatially stationary features of the flowfield were examined using hot-wire anemometry. Two apparently different flowfields were found in the boundary layer downstream of the actuator array. When the orifice was normal to the mean flow direction, the boundary layer was characterized by a wakelike region in the lee of the jet due to a blockage effect. When the orifice was aligned with the mean flow direction, the flow structure was consistent with the presence of longitudinal vortices embedded in the boundary layer.

I. Introduction

A JET issuing into a crossflow exhibits a rich and complex structure as the fluid from the two streams meet and interact. The basic flowfield is relevant to a wide variety of applications, including plume dispersion, gas-turbine wall cooling, reaction control for missiles, and transition from thrust-supported to wingborne flight of a vertical/standard takeoff and landing aircraft.[1] Arguably the most interesting feature of a jet issuing into a crossflow is the counter-rotating vortex pair that is formed from the crossflow interaction. If the jet trajectory and the vortex pair remain confined to the boundary-layer region of the flow, then the jet/boundary-layer interaction has an effect similar to a passive vortex generator. The vortex pair transports high-momentum fluid at the edge of the boundary layer to the near-wall region, creating a fuller velocity profile that is better resistant to separation.

Johnston and Nishi[2] proposed the idea of a steady jet in a crossflow, or vortex generator jet, as a flow control device. Their original idea suggested that skewing and inclining the jet relative to the incoming flow would create a dominant single-sign vortex. This initial study spawned a series of subsequent studies[3–5] where various skew and inclination angles for the jet were explored, the scale of the vortex was measured, and the effect on the boundary-layer structure was evaluated. For example, Compton and Johnston[3] showed that the flowfield downstream of the vortex generator jet exhibited characteristics similar in nature to the flowfield downstream of a weak solid vortex generator. In recent applications of this concept, studies by Bons et al.[6] and Rivir[7] have demonstrated that vortex generator jets are effective in delaying boundary-layer separation on gas-turbine compressor blades.

Although the vortex generator jet studies have shown that steady blowing can be effectively employed as a flow control device, unsteady blowing has been shown to produce similar control results at significantly lower flow rates. Recently, oscillatory jets placed upstream of the separation point on a bluff body have shown a remarkable ability to control the separated flow.[8] Moreover, the power required to effect control was found to be over an order of magnitude less than the power required to achieve the same control effect with a steady jet. In a study by Seifert et al.[9] on a NACA 0015 airfoil, oscillatory blowing (with a steady component) was used to increase the lift coefficient by 64% at angle of attack just before stall. In addition, the drag was reduced with the drag coefficient reaching a value as low as 28% of its base value. More recently, a study by Magill and McManus[10] used pulsed vortex generator jets to control separation on laboratory-scale aircraft wings at poststall angles of attack. By the use of eight discrete jets along the full span, a modest increase of 7% was observed in the lift coefficient.

A similar, and possibly more effective, control can be achieved with zero-net-mass-flux oscillatory blowing, that is, a synthetic jet. Smith et al.[11] and Amitay et al.[12] have used synthetic jet control on an airfoil to prevent boundary-layer separation and, hence, prevent stall at high angles of attack. In these studies, a 24% thick airfoil was used with a synthetic jet slot that could be positioned at any location between the airfoil leading edge and the maximum thickness location (25% chord). With control, stall was delayed to an angle of attack 10 deg in excess of the stall angle without control. As a consequence, large gains in lift and dramatic reductions in drag were realized.

There is no question that there is a clear link between unsteadiness in a jet issuing into a crossflow and the efficiency of the jet for flow control. To understand the flow physics of these unsteady jets and the mechanism by which they effect control, it is important to study in isolation the various important features of these jets. The purpose of the present investigation is to explore the spatially stationary interaction between an array of synthetic jets and a turbulent crossflow boundary layer. Two array configurations are investigated that differ only in the orientation of the synthetic jet orifice relative to the freestream.

II. Experimental Setup

The experiments were conducted in a blowdown facility where high-pressure air is exhausted from a rectangular duct over a flat plate (Fig. 1). The lower wall of the duct extended beyond the duct exit plane to form the flat-plate test surface. The actuator array and mounting frame were located approximately 76.2 ± 0.8 mm downstream of the duct exit. The tunnel velocity was set by manually opening a valve until the pressure in the settling chamber upstream of the duct reached a predetermined value, which corresponded to a known velocity at the duct exit. In these tests, the freestream velocity was nominally 9.1 ± 0.1 m/s. The boundary layer on the flat plate upstream of the actuators was fully turbulent after undergoing transition within the duct. Detailed velocity profiles in the boundary layer are presented in the next section.

The actuator array included three individual synthetic jet actuators. The actuators were assembled to form a single block that was installed in the flat plate. Each actuator was driven by piezoelectric diaphragm similar in design to the actuators of Smith and Glezer.[13] In the current design, the actuator orifice was rectangular with an aspect ratio of 45. The height h of the orifice was 0.51 ± 0.02 mm and the length w was 22.90 ± 0.02 mm. The peak output of the actuators occurred at a driving frequency of $f_e = 1800$ Hz, and, for all measurements, the amplitude of the driving signal was $100V_{p-p}$.

Received 6 November 2001; revision received 7 June 2002; accepted for publication 25 June 2002.

*Assistant Professor, Department of Mechanical Engineering, P.O. Box 3295; drsmith@uwyo.edu. Senior Member AIAA.

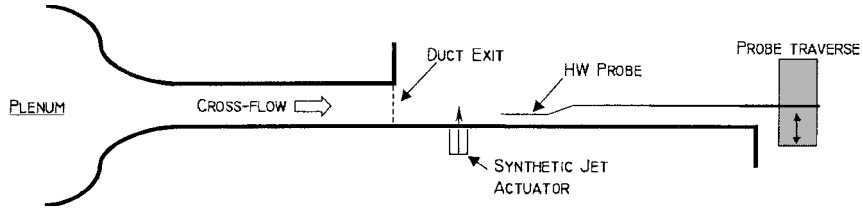

Fig. 1 Schematic of the flat-plate test facility.

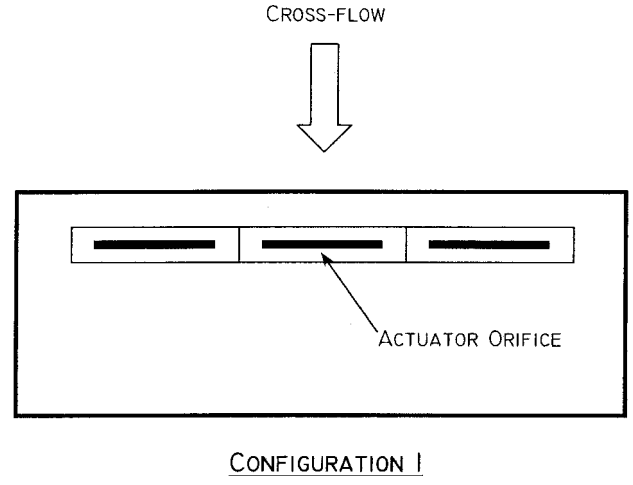

Spanwise configuration

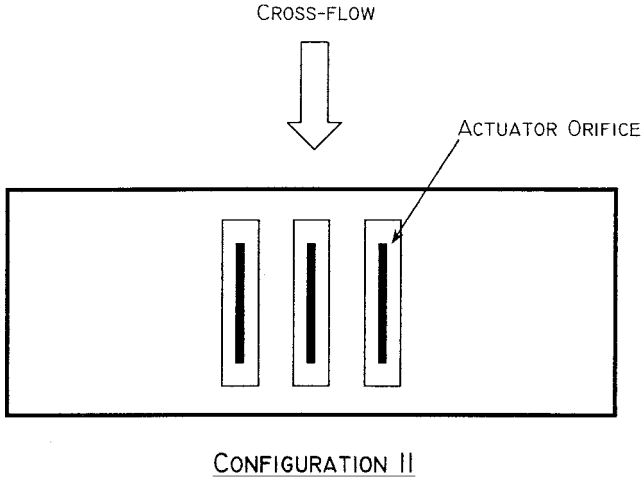

Streamwise configuration

Fig. 2 Schematics of the actuator configurations.

Two actuator array configurations were investigated. In the first configuration, the major axes of the actuator orifices were coincident and oriented perpendicular to the crossflow direction (spanwise configuration, Fig. 2). The distance between the geometric centers of the rectangular orifices was 33.0 ± 0.8 mm. In the second configuration, the three actuators were stacked together such that the major axes of the orifices were parallel and, when installed in the test plate, were also parallel to the crossflow direction (streamwise configuration; Fig. 2). In this configuration, the distance between the orifice centers was 10.2 ± 0.8 mm. For both configurations, the centerline of the actuator array was coincident with the duct centerline.

Detailed mean and root-mean-square velocity profiles in the boundary layer and in the synthetic jet were obtained using a single-sensor hot wire probe. A static calibration of the hot wire, based on King's law, was obtained by placing the probe in the freestream at the duct exit. Calibrations were made before each run and compared with earlier calibrations. The instrument uncertainty in the velocity measurements was found to be ± 0.1 m/s. In terms of U/U_∞, this uncertainty gives a maximum relative uncertainty of $\pm 4.8\%$.

Streamwise, x, and spanwise, z, distances were accurate to ± 0.8 mm. These distances were normalized by the relevant orifice dimension in the same direction. For example, in the spanwise configuration, the streamwise distance was normalized by the orifice height h, and the spanwise distance was normalized by the orifice length w. For all profile measurements, the cross-stream distance y was accurate to ± 0.4 mm and was normalized by the upstream boundary-layer thickness δ_0.

The integral parameters δ^*, θ, and H were determined from a numerical integration of the velocity profiles. The percentage error in the estimation of δ^*, θ, and H due to the uncertainty in the velocity measurement is 18, 16, and 34%, respectively.

III. Interaction of the Jets with the Crossflow

The focus of this work is on building an understanding for the statistically stationary velocity field resulting from the interaction of a synthetic jet and a turbulent boundary layer. A synthetic jet is the result of an inherently unsteady flow phenomenon occurring in the near field of the actuator orifice. For the jet formation process to appear stationary relative to the incoming boundary layer, it is desired to have a jet formation frequency that is appreciably higher, for example, by an order of magnitude, than a characteristic frequency associated with the boundary layer. The ratio of these frequencies then gives a measure of the apparent steadiness of the interaction. To this end, one can compare the jet formation frequency f_e with a characteristic frequency of the boundary layer, U_∞/δ_0. In the current experiment, this ratio exceeded 60, indicating that the interaction between the jet and the boundary-layer flow may be thought of as quasi-steady. Note that the specific formation frequency is chosen to optimize the actuator performance rather than couple to, or excite, specific frequencies within the boundary layer.

A. Characterization of Actuator Array and Boundary-Layer Flows

Smith and Glezer[13] characterized the formation of synthetic jets in terms of four parameters, each associated with the formation of vortex rings. These parameters were the stroke length L_0/h, the Reynolds number based on the impulse per unit width Re_{I_0}, the formation frequency f_e, and the duty cycle. The latter two parameters are specific to the time-periodic formation of vortex rings and for the current study were constant. The stroke length was obtained from

$$L_0 = \int_0^{T/2} u(t)\,\mathrm{d}t$$

and the Reynolds number Re_{I_0} was defined as $I_0/\mu h$, where

$$I_0 = \rho h \int_0^{T/2} u^2(t)\,\mathrm{d}t$$

Here, $u(t)$ is the instantaneous velocity at the jet orifice. For comparison with Smith and Glezer, the stroke length L_0/h for the current synthetic jets was 12.5, and the Reynolds number based on the impulse per unit width Re_{I_0} was 1.35×10^4.

For both configurations, the time-averaged distributions of the streamwise velocity component were measured across the three actuators in the absence of a crossflow. From these profiles, the actuator performance and the uniformity in output among the individual actuators was evaluated. Figures 3a and 3b show the velocity profiles, measured at $y/h = 10$, for the spanwise and streamwise configurations, respectively. In the spanwise configuration, the centerline

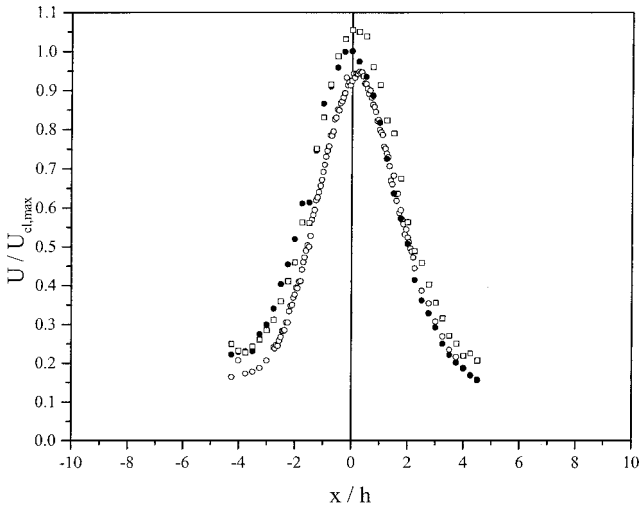

a) Spanwise configuration: ○, $z/w = -1.4$; ●, $z/w = 0$; and □, $z/w = 1.4$

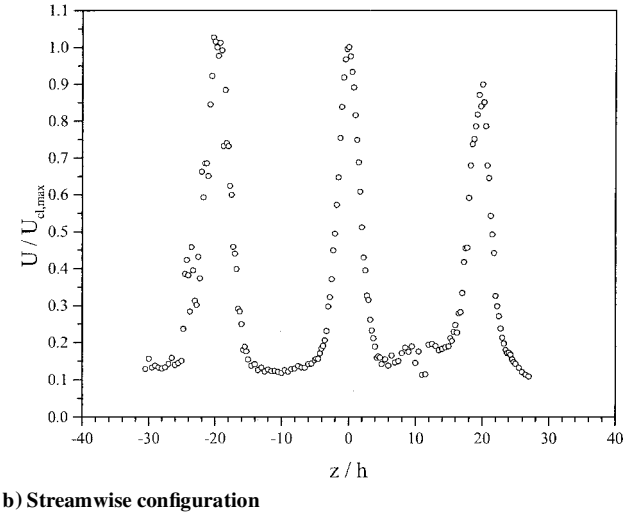

b) Streamwise configuration

Fig. 3 Time-averaged velocity profiles at $y/b = 10$ for the actuator arrays in the absence of a crossflow.

velocities were within ±10% of each other. For the streamwise configuration, the variation in the centerline velocity between the three actuators was ±5%. Note that for the present spacing between actuators and at this height ($y/h = 10$), there appeared to be no merging or interaction of the jets.

To facilitate comparisons with steady jets in a crossflow, a jet-to-freestream velocity ratio r was defined as

$$r = \left(\rho_j U_0^2 \big/ \rho_\infty U_\infty^2\right)^{\frac{1}{2}} = U_0/U_\infty$$

where U_0 is an average orifice velocity (defined as $L_0 f_e$). For both configurations, U_0 was nominally 11.3 ± 0.1 m/s and the velocity ratio was $r = 1.2$. The measurements of Smith and Glezer[13] for a synthetic jet without a crossflow show that U_0 is slightly larger than, but approximately equal to, the centerline mean jet velocity measured in the jet at $y/h = 10$. Hence, U_0 is a not unreasonable choice for a characteristic velocity of the jet.

To characterize the incoming boundary layer and to evaluate apparent modifications to the boundary layer due to the mounting of the actuator array into the wall, mean velocity profiles in the boundary layer at seven streamwise locations along the centerline of the test surface were obtained. To characterize the mean two dimensionality of the flow, off-centerline profiles were obtained.

The mean velocity profiles at the extreme upstream ($x = -20.3$ mm) and downstream ($x = 102$ mm) positions are shown in Fig. 4. The mean velocity profiles are shown in inner variables; τ_w was estimated using the Clauser chart method. Note that the boundary layer in the duct was exposed to a favorable pressure gradient,

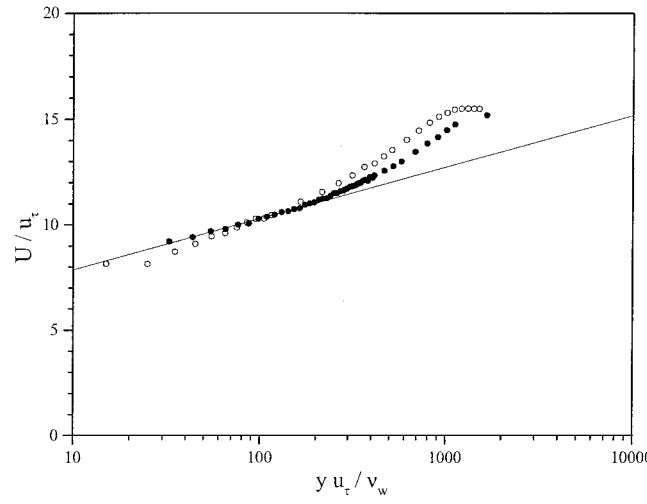

Fig. 4 Mean streamwise velocity profiles in the boundary layer shown with inner variables (synthetic jet inactive); the straight line is the logarithmic law of the wall: ○, $x/h = -40$ and ●, $x/h = 200$.

and, as the boundary layer began to adjust to the zero-pressure-gradient downstream of the duct exit, it initially exhibited only a small logarithmic region. Farther downstream, the mean velocity profile exhibited a distinct logarithmic region, indicating that the boundary layer was uninfluenced by the exposed, undriven actuator orifices. Some cross-span variation in the mean velocity profiles was observed in the off-centerline profiles, but within the narrow region around the centerline where the velocity measurements were made, the boundary layer was nominally two dimensional in the mean. The boundary-layer thickness δ_0, estimated from the mean velocity profile at $x = -20.3$ mm, was 28.7 mm. The corresponding integral parameters at the same location were $\delta_0^* = 4.2$ mm, $\theta_0 = 2.9$ mm, and $H_0 = 1.44$.

B. Actuator Array with Crossflow: Spanwise Configuration ($\beta = 90$ deg)

For the spanwise configuration, mean streamwise velocity profiles were measured at 13 locations along the interaction centerline. These profiles are shown in Figs. 5a and 5b. In these profiles, the farthest upstream profile ($x/h = 30$) was located downstream of the last measurement position where phase-coherent fluctuations (at the actuator frequency) were detected; that is, the mean flow was stationary. Figure 5a shows the velocity profiles for $30 \le x/h \le 60$. For $x/h \le 50$, a velocity overshoot is observed in the profiles, starting near $y/\delta_0 = 0.2$ and appearing higher in the boundary layer at successive downstream locations. This overshoot is consistent with a strong, apparently steady jet issuing from the wall that is bent downstream by the crossflow. In addition, the movement of the overshoot away from the wall further suggests that the velocity field in this region possesses a nonnegligible positive component normal to the wall. The normal wire probe used in these measurements can not resolve velocity components and, consequently, overestimates the streamwise velocity in this region. From the three profiles between $30 \le x/h \le 40$, one observes that the jet blocks the incoming boundary-layer flow, and the shape of the velocity profile below $y/\delta_0 = 0.1$ suggests a region of reverse flow. By $x/h = 45$, the mean velocity profile near the wall indicates that the region of separated flow has closed. Farther downstream, in the lee of the jet, fluid is drawn in along the wall from the sides of the jet; the fluid meets at the plane of symmetry and creates a local peak in the velocity profile near the wall. At $x/h = 45$, the development of a wake region in the boundary layer is observed and is due presumably to the blockage effected by the synthetic jet. For the profiles shown in Fig. 5a, the velocity distribution near the wall is less full everywhere than the upstream profile (open symbols). Figure 5b shows the velocity profiles for $70 \le x/h \le 200$. Here, the profiles are characterized by an expanding interaction wake and by the development of a wall-jet-like character near the wall where high-momentum fluid is swept in from off center.

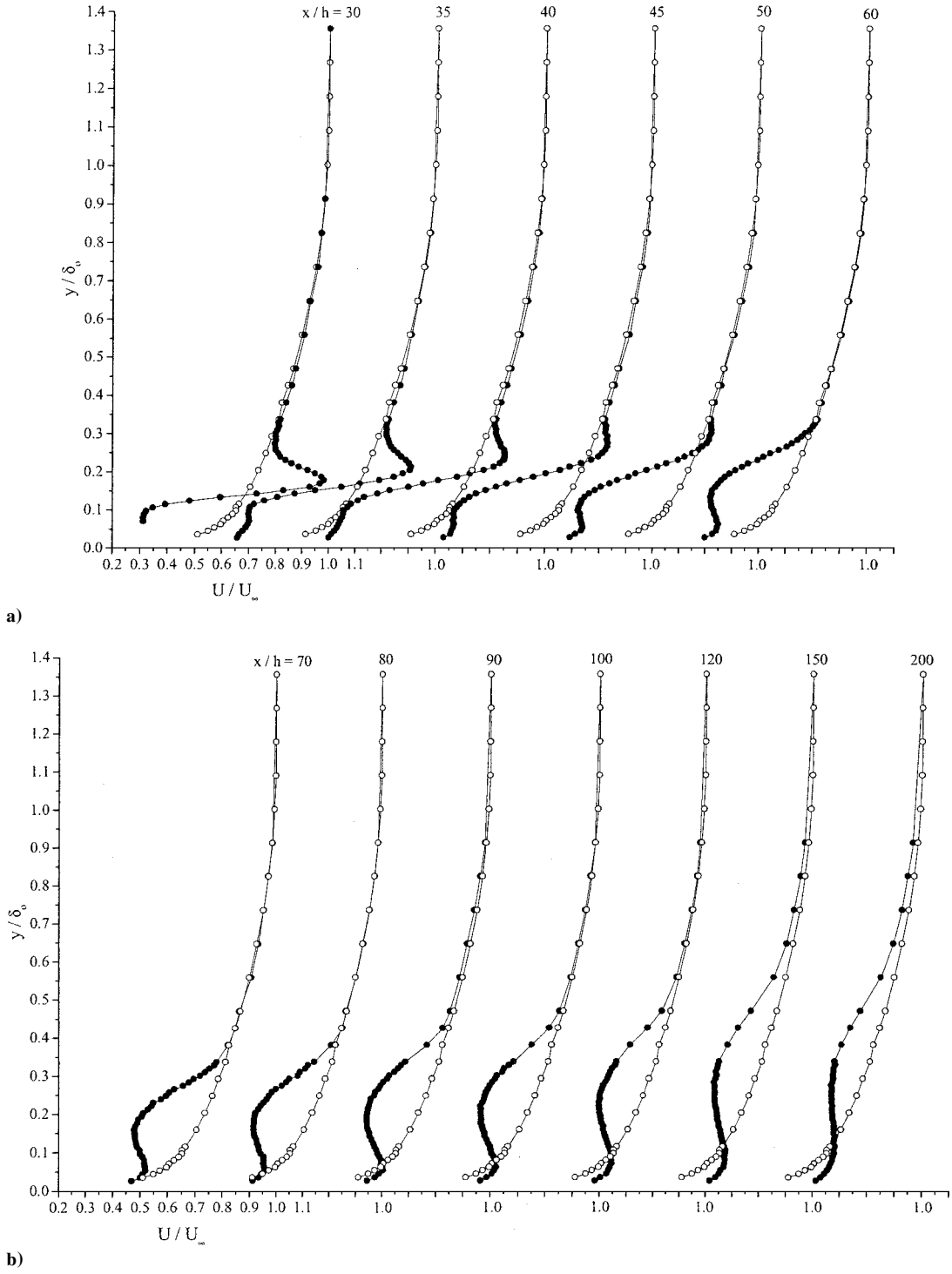

Fig. 5 Mean streamwise velocity profiles along the interaction centerline for successive streamwise locations in the spanwise configuration: a) $x/h = 30$–60 and b) $x/h = 70$–200; for clarity, the profiles are staggered along the horizontal axis by four major axis units; for comparison, the upstream boundary-layer profile is shown as ○ at each streamwise position.

For $x/h \geq 80$, the velocity defect in the wake grows to occupy a larger portion of the boundary layer, is displaced away from the wall by the wall-jet effect, and, by the last measurement station, occupies the region $0.1 \leq y/\delta_0 \leq 0.5$. By $x/h = 70$, the velocities near the wall have recovered to the upstream levels, and the fuller velocity profile near the wall first observed at $x/h = 80$ grows steadily with streamwise distance. By the last measurement station, the near-wall profile is still fuller than the upstream profile and has shown no indication of relaxing.

Centerline profiles of the streamwise turbulence intensity are shown in Figs. 6a and 6b. An elevated turbulence level, due to the synthetic jet, is evident in all profiles. The peak turbulence intensity near $y/\delta_0 = 0.15$ increases with streamwise distance until $x/h = 40$. This peak in the profile corresponds to a region of high mean shear (Fig. 5a), where turbulence production is expected to be high. The drop in the turbulence levels near the wall can be attributed to the separated flow in this region. Note that the profile at $x/h = 45$ suggests that the region of separated flow in the lee of the jet closes between $40 < x/h < 45$. At subsequent downstream locations, both the local peak in the turbulence intensity and the level of the turbulence intensity near the wall decay with streamwise distance. Turbulent diffusion broadens the peak created by the synthetic jet and the interaction wake. Turbulent diffusion also increases turbulence levels in the outer half of the boundary layer where the turbulence acts to fill in

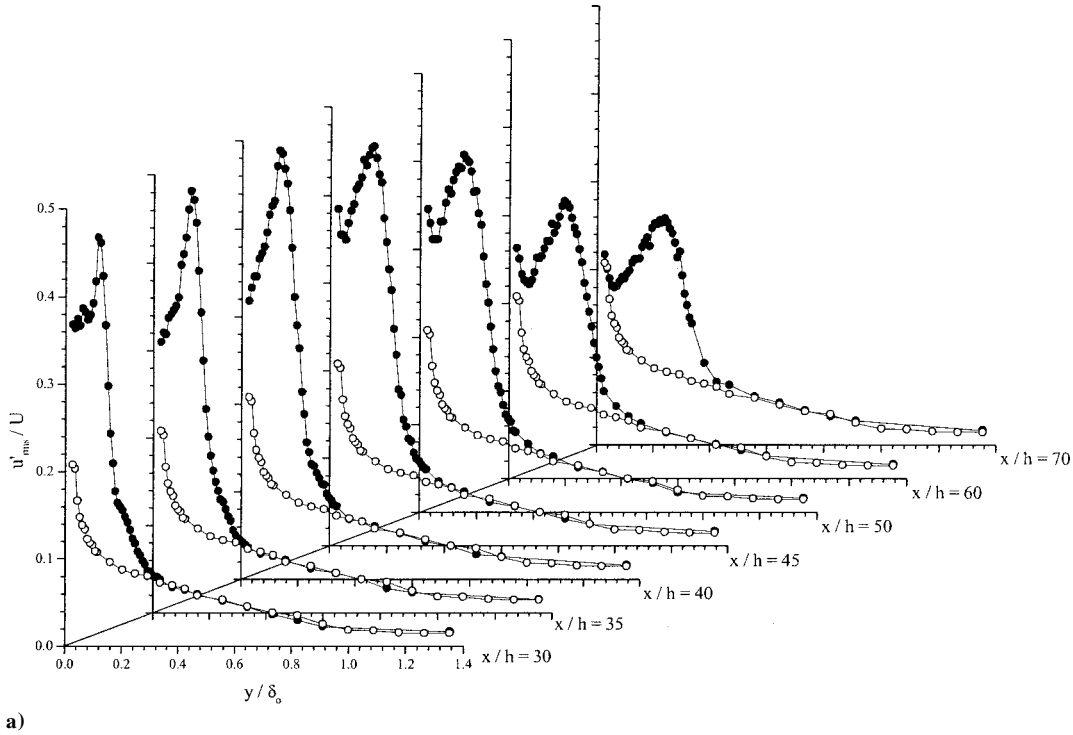

a)

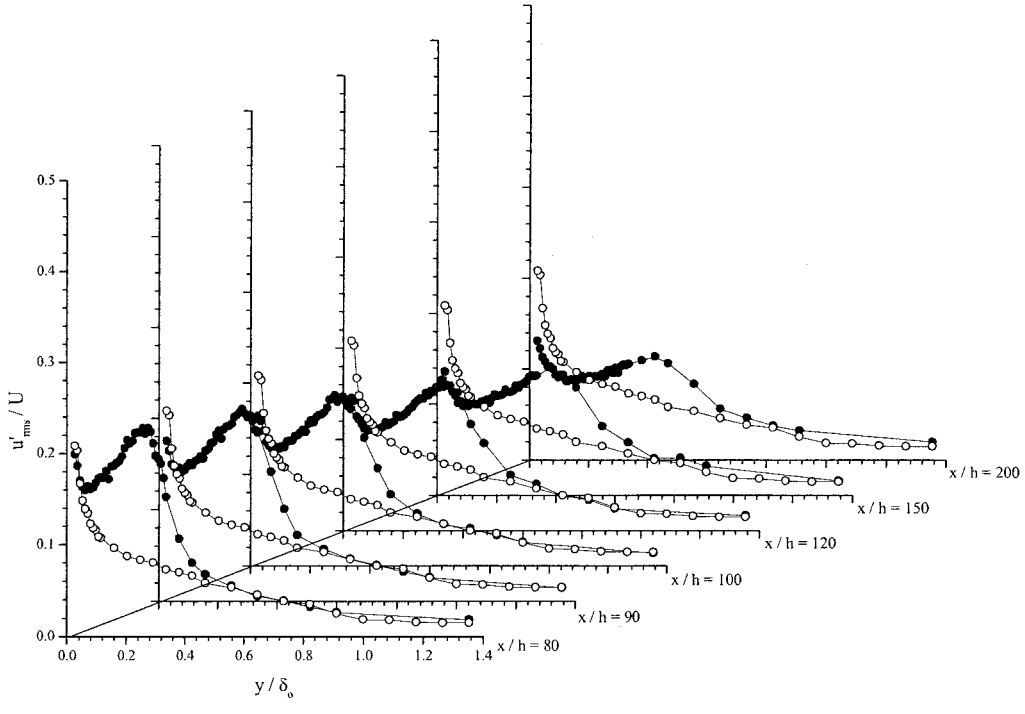

b)

Fig. 6 Profiles of the streamwise turbulence intensity at successive locations along the interaction centerline in the spanwise configuration: a) $x/h = 30$–70 and b) $x/h = 80$–200; for comparison, the upstream boundary-layer profile is shown as ○ at each streamwise position.

the velocity profile gradually. At the last downstream measurement location, the local peak in the turbulence intensity is still decaying and moving away from the wall, whereas the turbulence level at the wall appears to be constant with streamwise distance. At $x/h = 80$, where the mean velocity at the wall begins to overshoot the upstream level, the beginning of a drop in the relative turbulence intensity below the upstream levels is observed. This trend is due to the higher mean velocity at the wall, and one can conclude that the absolute fluctuation levels are likely comparable with the upstream levels.

Figure 7 shows the variation in δ^*, θ, and H along the interaction centerline for the spanwise configuration. Each quantity has been nondimensionalized by its corresponding upstream value. The displacement thickness, after an initial increase in excess of 45%, remains approximately constant over the streamwise extent of the measurement domain. In contrast, the momentum thickness increases monotonically for $x/h > 40$ and appears to be reaching an asymptotic limit at the end of the measurement domain. The combined effect of δ^* and θ is reflected in the streamwise trend in the shape factor. Initially, H is 40% greater than the upstream value, but it decreases steadily with streamwise distance and by the end of the measurement domain has returned to a value typical of a turbulent boundary layer at this Reynolds number, that is, 1.44.

Mean velocity profiles for off-centerline positions were obtained at seven streamwise locations. At two streamwise positions, $x/h = 50$ and 200, detailed off-centerline profiles were obtained with profiles at intervals of $\Delta z/w = 0.07$ from the centerline of the

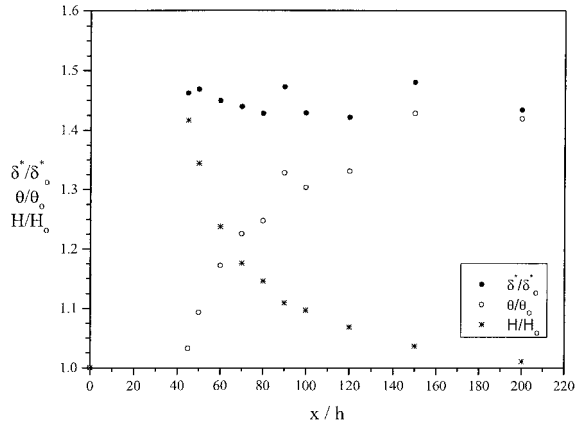

Fig. 7 Streamwise variation of the integral parameters along the interaction centerline for the spanwise configuration.

array to $z/w = -0.42$ (Figs. 8a and 8b). A profile at $z/w = -0.76$, midway between two actuators, is also included in Figs. 8a and 8b. At $x/h = 50$, the separated region in the lee of the jet has closed, but the blockage effect of the jet is still observed up to a height of $y/\delta_0 = 0.3$ and out to a spanwise position of $z/w \leq -0.28$. The mean velocity profiles at $z/w = -0.35$ and -0.42 suggest that the blockage by the jet is causing a channeling of fluid between adjacent jets with an increase in the mean velocity near the wall. The profile at $z/w = -0.76$, however, appears almost unchanged from the upstream profile. Note that, at this streamwise location, the wall-jet behavior is only observed along the centerline of the interaction.

At $x/h = 200$ (Fig. 8b), the wall-jet-like behavior is most pronounced along the interaction centerline, but is apparent in the profiles out to $z/w = -0.28$. By comparison with the centerline profiles, the off-center mean velocity profiles exhibit lower velocities near the wall. That the wakelike behavior is only observed in the velocity profiles out to $z/w = -0.28$ suggests that the aspect ratio of the jet changes quickly with downstream distance. Consequently, the

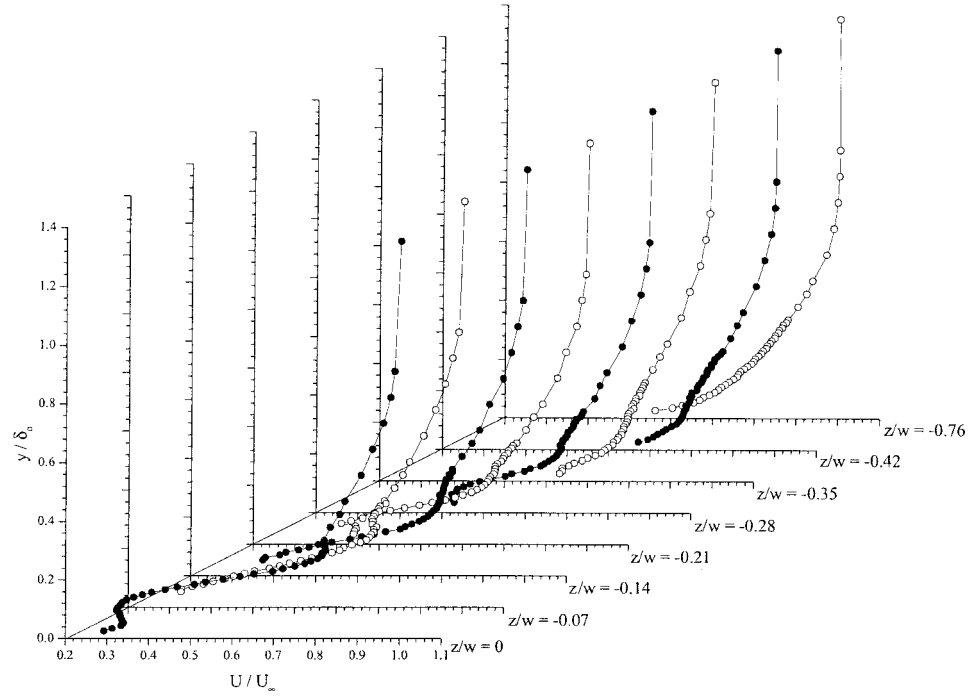

a) *x/h* = 50

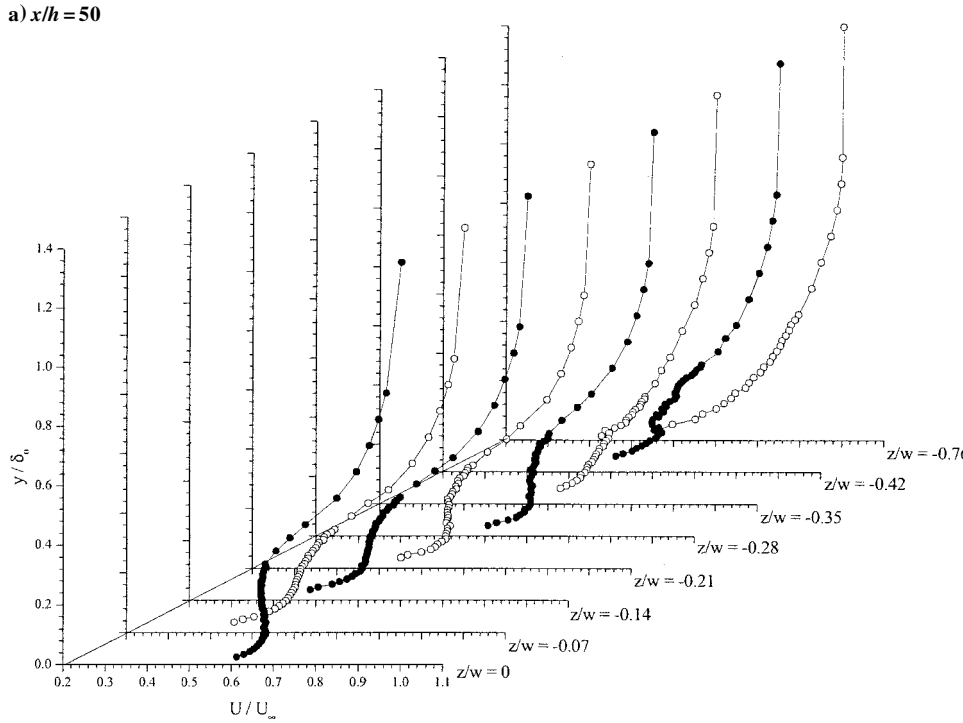

b) *x/h* = 200

Fig. 8 Spanwise variation in the mean streamwise velocity profiles at two streamwise positions downstream of the actuator in the spanwise configuration.

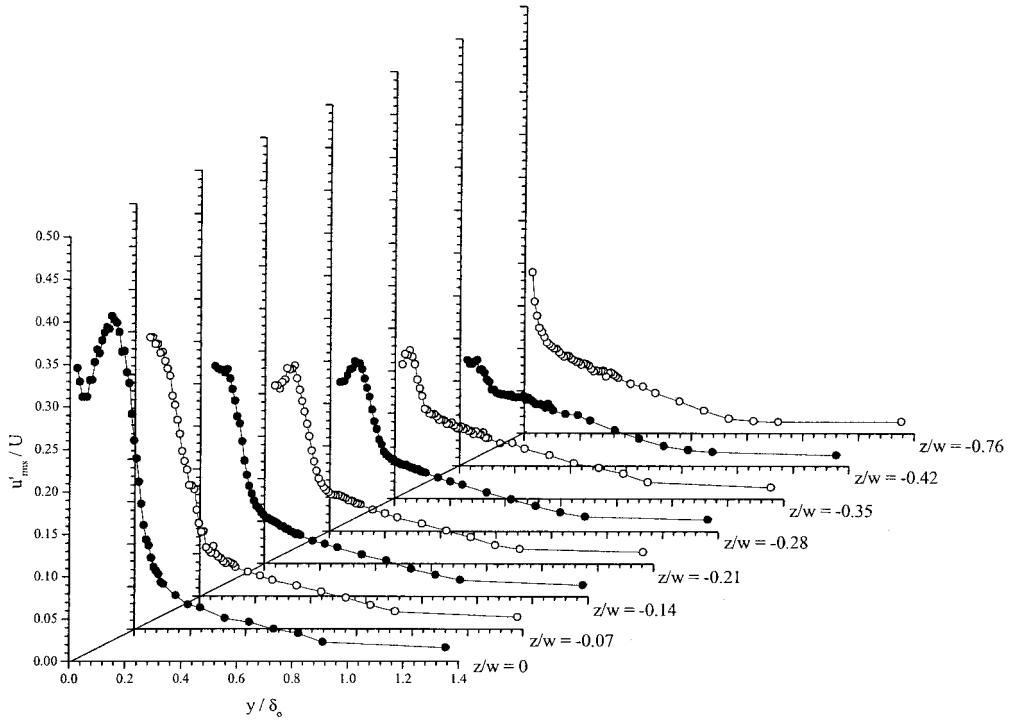

a) $x/h = 50$

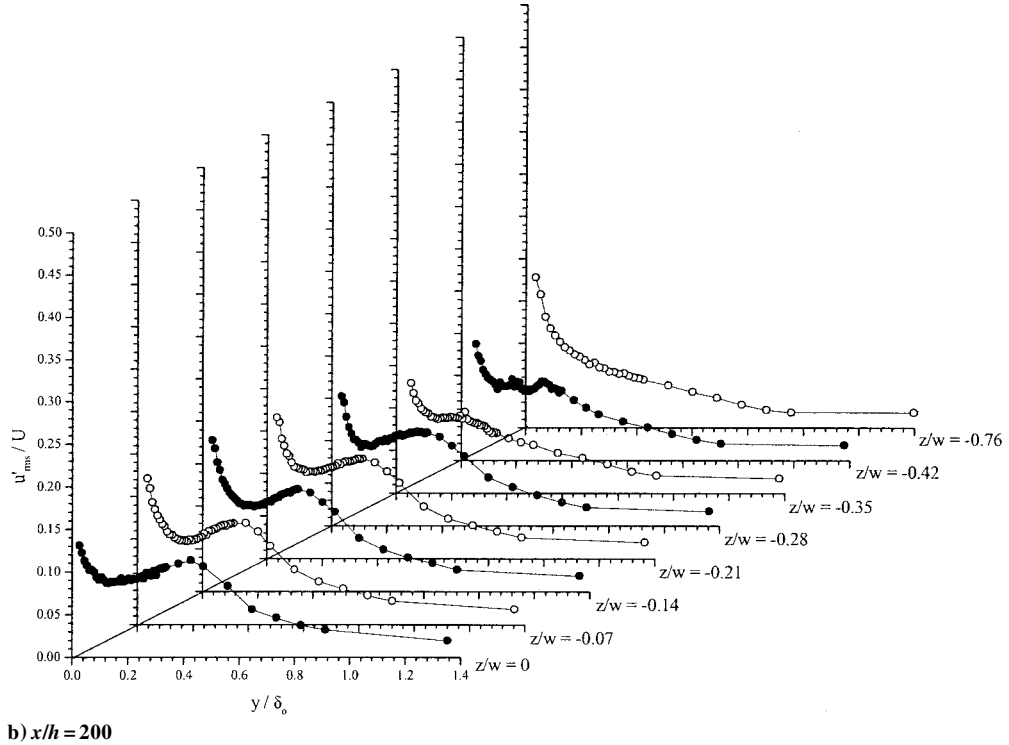

b) $x/h = 200$

Fig. 9 Spanwise variation in the streamwise turbulence intensity profiles at two streamwise positions downstream of the actuator in the spanwise configuration.

flow between the actuators ($z/w = -0.76$) remains unaffected by the synthetic jets to either side. However, the channeling effect due to the blockage and the influx of fluid to the lee region of the jet, due to low pressure there, is observed in the velocity profiles near the edges of the jet ($z/w = -0.35$ and -0.42).

The corresponding off-centerline turbulence intensity profiles are shown in Figs. 9a and 9b. At $x/h = 50$ (Fig. 9a), the near-wall turbulence intensity decays monotonically away from the centerline. The near-wall peaks in the profiles occur at positions where the mean velocity profiles show the highest shear. This region of high shear is closer to the wall as the distance from the centerline increases, and the peaks in the turbulence intensity profiles follow the same trend. Beyond $y/\delta_0 = 0.3$, the turbulence intensity profiles at all spanwise locations appear similar and mostly unchanged from the upstream boundary-layer profile. At $x/h = 200$ (Fig. 9b), the profiles are remarkably similar across the span with a slight attenuation in the peak intensity in the $z/w = -0.35$ and -0.42 profiles. Also, as observed in the mean velocity profiles at $z/w = -0.76$, the turbulence intensity profiles at this location are unaffected by the jets.

Integral parameters were obtained from the velocity profiles taken at the cross-span locations, $x/h = 50$ and 200. Similar trends were observed at both streamwise positions, and only the $x/h = 200$

trends are shown in Fig. 10. Both δ^* and θ decrease away from the interaction centerline, reaching a minimum at $z/w = -0.4$ and -0.3, respectively. At the upstream position, δ^* decreases more than θ, resulting in a decrease in H along the span. At the downstream position, the decreases in δ^* and θ are comparable, and H is relatively constant along the span. In addition, at this downstream position, the integral parameters far off of the centerline have taken values approximately equal to the upstream values, suggesting that in this off-centerline region the boundary layer is uninfluenced by the synthetic jet.

C. Actuator Array with Crossflow: Streamwise Configuration ($\beta = 0$ deg)

For the streamwise configuration, profiles of the mean streamwise velocity in the boundary layer were obtained at six locations along the interaction centerline (Fig. 11). The main features of these profiles are the wall-jet appearance of the near-wall profile and the interaction wake that dominates a large portion of the outer boundary layer. The wall-jet profile shape appears at $x/h = 2$, where high momentum fluid has filled the low-pressure region near the wall in the lee of the jet. As a consequence, the velocity profile is decidedly fuller than the upstream profile (open symbols) with higher mean shear near the wall. In contrast to the spanwise configuration where the fuller velocity profiles near the wall developed with streamwise distance, here the fuller profiles appear to be diminishing with streamwise distance. Moreover, although an overshoot still appears in the profiles beyond $x/h = 4.0$, the velocity closest to the wall is unchanged from the upstream value. The interaction wake evolves rapidly in the lee of the jet and, by the last measurement station, has grown to encompass the entire upper 80% of the boundary layer and possibly penetrates beyond the edge of the boundary layer at this station. Interestingly, the features of these profiles bear a remarkable resemblance to the mean velocity profiles obtained by Andreopoulos and Rodi[14] ($r = 2$) and Crabb et al.[15] ($r = 1.15$) downstream of a steady circular jet in crossflow. Note that in these studies, the flow is presumably dominated by a streamwise aligned counter-rotating vortex pair.

The centerline turbulence intensity profiles for the streamwise configuration are shown in Fig. 12. The turbulence intensity near the wall at $x/h = 1.0$ is significantly attenuated relative to the upstream level. The elevated turbulence level in the synthetic jet is apparent at a height of $y/\delta_0 = 0.4$ in the early profiles, and, due to a higher relative mean velocity at this height in the boundary layer, the magnitude of the peak in these profiles is lower than in the spanwise configuration. Moving downstream, the peak diffused over an increasing portion of the boundary layer, and by the last measurement station ($x/h = 5.0$), the turbulence intensity was almost uniform between $0.2 < y/\delta_0 < 0.8$. Note that as the turbulence levels in the middle and upper parts of the boundary layer decreased and broadened, the fluctuation level near the wall increased. This observation is consistent with the high shear observed near the wall in the mean velocity profiles and the expected increase in production of turbulent energy that would come with the high shear. As observed in the mean velocity near the wall, the near-wall turbulence intensity at the downstream positions is quite close to the upstream intensity level.

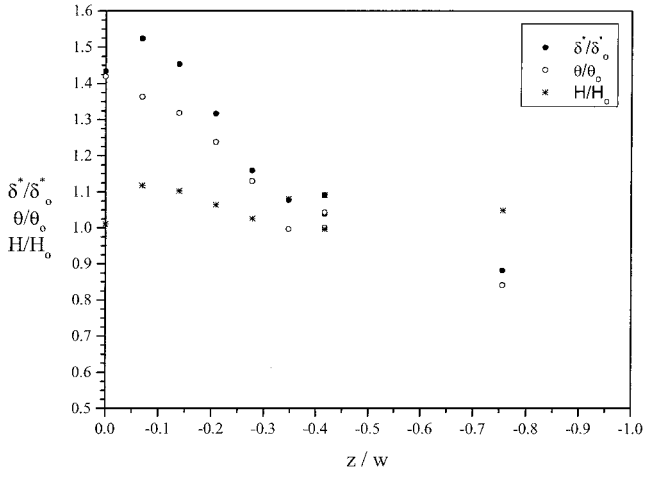

Fig. 10 Cross-span variation of the integral parameters at $x/h = 200$ and corresponding to the velocity profiles in Fig. 8.

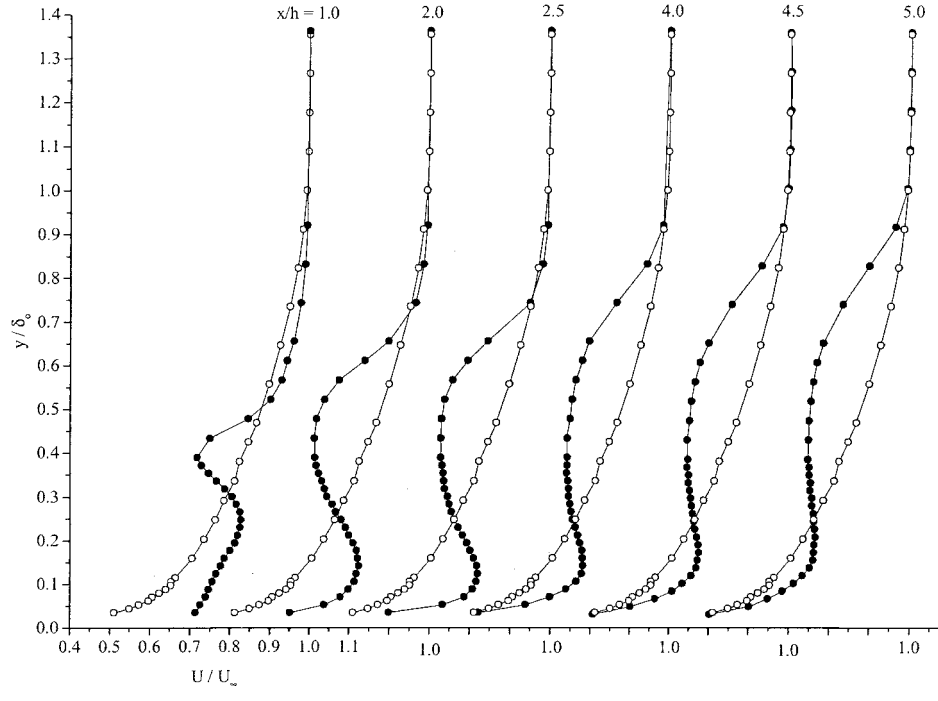

Fig. 11 Mean streamwise velocity profiles along the interaction centerline in the streamwise configuration; for clarity, the profiles are staggered along the horizontal axis by three major axis units; for comparison, the upstream boundary-layer profile is shown as ○ at each streamwise position.

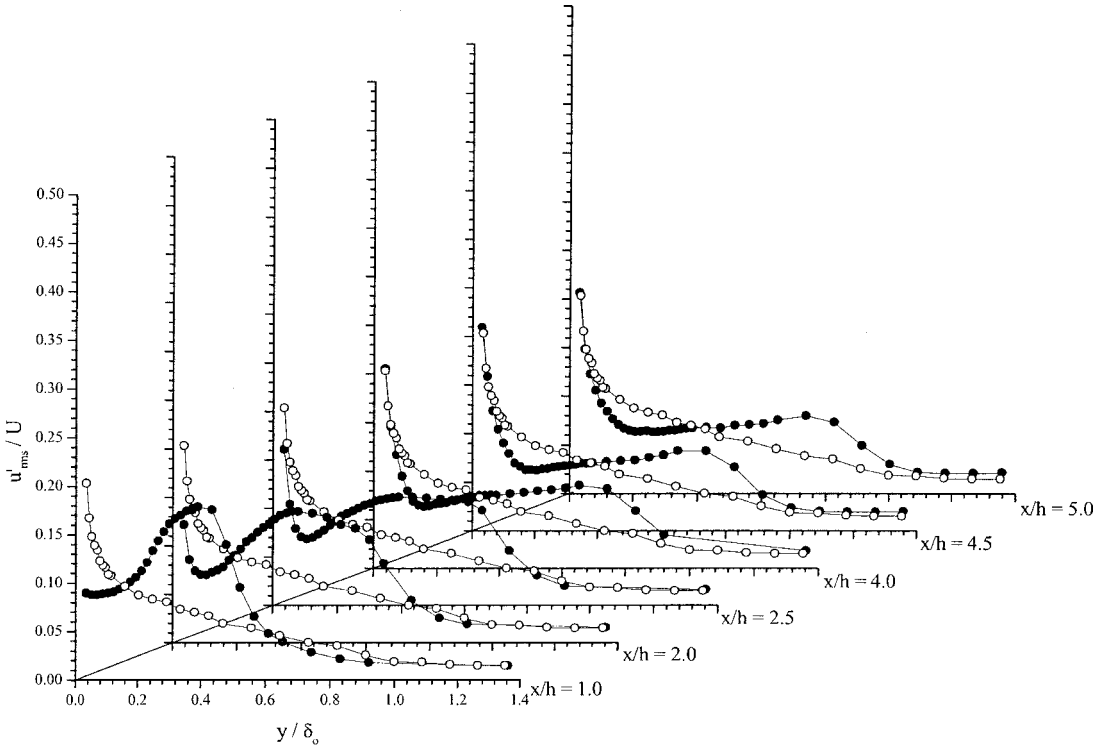

Fig. 12 Profiles of the streamwise turbulence intensity along the interaction centerline in the streamwise configuration; for comparison, the upstream boundary-layer profile is shown as ○ at each streamwise position.

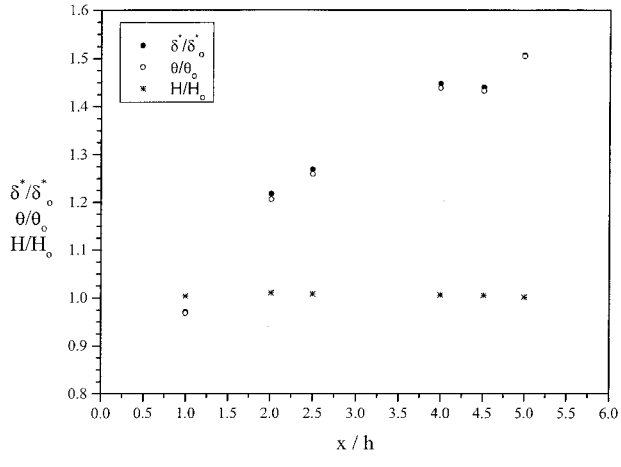

Fig. 13 Streamwise variation of the integral parameters along the interaction centerline for the streamwise configuration.

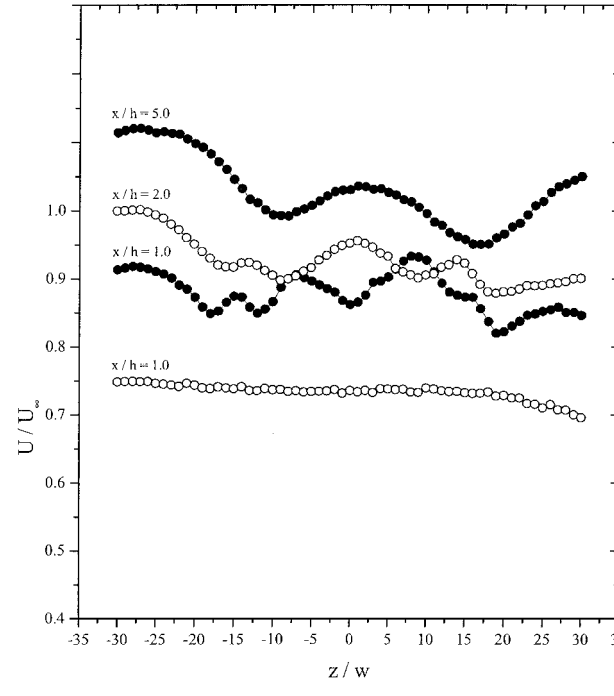

Fig. 14 Mean streamwise velocity variation in the cross-span direction at a height of $y/\delta_0 = 0.19$ for the streamwise configuration; cross-span velocity variation in the boundary layer without the actuators is shown in the lower profile of ○; for clarity, the profiles are staggered along the vertical axis by one unit. (Note that the actuators are located at $z/w = -20, 0$, and 20.)

Figure 13 shows the variation in δ^*, θ, and H along the interaction centerline for the streamwise configuration. In contrast to the spanwise configuration, both δ^* and θ increase with streamwise distance, but at a rate that keeps H constant at a value approximately equal to that found for the upstream boundary layer.

Returning to the comparison made earlier with the steady jet in a crossflow, the presence of longitudinal streamwise vortices in a boundary layer typically creates spanwise undulations in the mean velocity at a given height in the boundary layer. Figure 14 shows spanwise profiles of the mean streamwise velocity at $y/\delta_0 = 0.19$ for three positions downstream of the actuator array. At $x/h = 1.0$, cross-span variations with relatively short wavelengths are observed and are likely due to a blockage of the boundary layer by the synthetic jets. By $x/h = 2.0$, the development of a longer wavelength undulation in the profile, which dominates farther downstream, is observed. The spanwise profile at $x/h = 5.0$ is consistent with the presence in the boundary layer of a pair of streamwise-aligned vortices. These vortices draw high-momentum fluid down in the boundary layer along the interaction centerline and lift low-momentum fluid away from the wall at $z/w = -10$ and 15. The spanwise scale of the vortex pair is approximately equal to the spanwise scale of the actuator array. This observation leads to speculation that the pair is the result of the interaction of the entire array with the boundary layer and not just one actuator. Moreover, the sense of rotation of the vortices would suggest that the off-center actuators may initiate the pair formation by starving the center actuator of fluid. This effect would create a low-pressure region at $z/w = 0$ that would

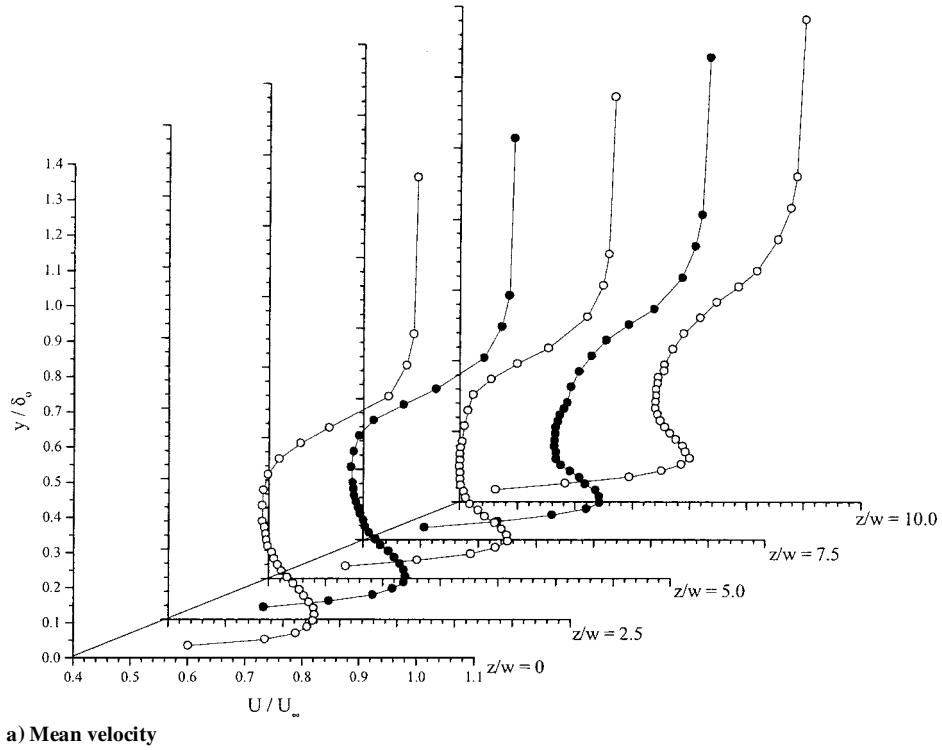

a) Mean velocity

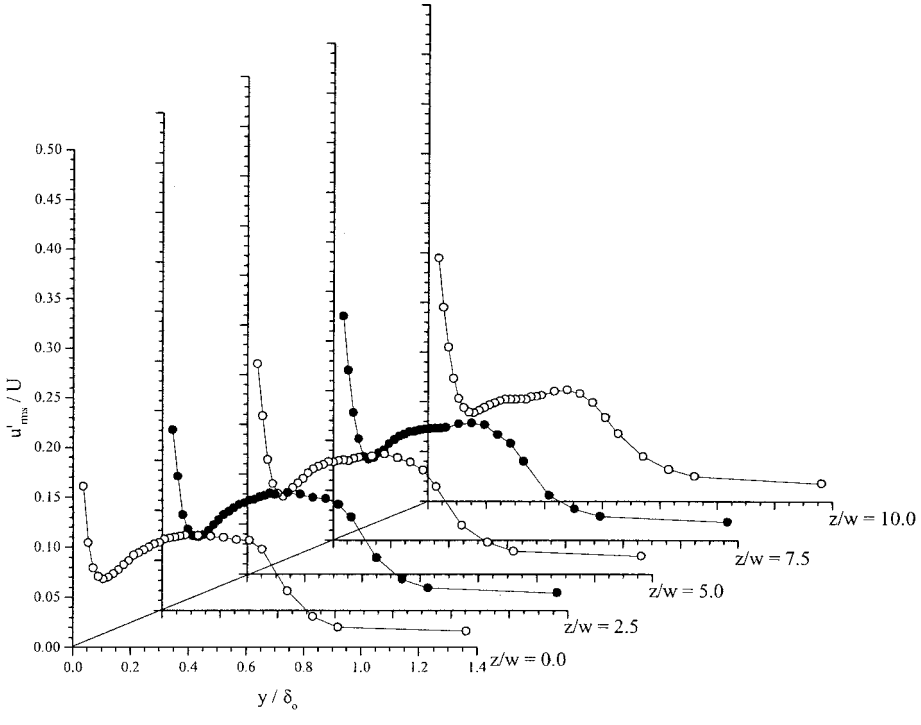

b) Streamwise turbulence intensity

Fig. 15 Spanwise variation in mean velocity and streamwise turbulence intensity profiles at *x/h* = 2.5 in the streamwise configuration.

subsequently lead to a downward motion of fluid and initiate the formation of the vortex pair.

To further investigate the off-centerline flowfield in the streamwise configuration, boundary-layer profiles were obtained at four off-center locations. In Figs. 15a and 15b, off-center mean velocity and turbulence intensity profiles are shown for $x/h = 2.5$, respectively. Profiles on both sides of the centerline were measured, but revealed no asymmetry in the interaction; consequently, profiles on only one side of the centerline are shown. Note that the off-centerline position $z/w = 10$ is midway between the centerline actuator and the neighboring actuator.

At $x/h = 2.5$ (Fig. 15a), the mean velocity profiles are uniform in appearance across the span with a wall-jet appearance near the wall that is slightly fuller at the centerline than it is at off-center positions. The spanwise extent of the jet/boundary-layer interaction has developed quickly in the lee of the jet. All profiles have a velocity defect between $y/\delta_0 = 0.1$ and 0.7 with the wake of the synthetic jet/boundary-layer interaction extending over 60% of the boundary-layer thickness at all spanwise positions. The uniformity in the mean velocity profiles is also observed in the turbulence intensity profiles for $y/\delta_0 > 0.15$ (Fig. 15b). As with the centerline turbulence profiles near the wall, the relative turbulence intensities off-center are lower in streamwise configuration than in spanwise configuration because of higher relative mean velocities in the boundary layer for this configuration. Note that, near the wall, the turbulence intensity increases as $z/w = 10$ is approached. Also, the dip in the profile

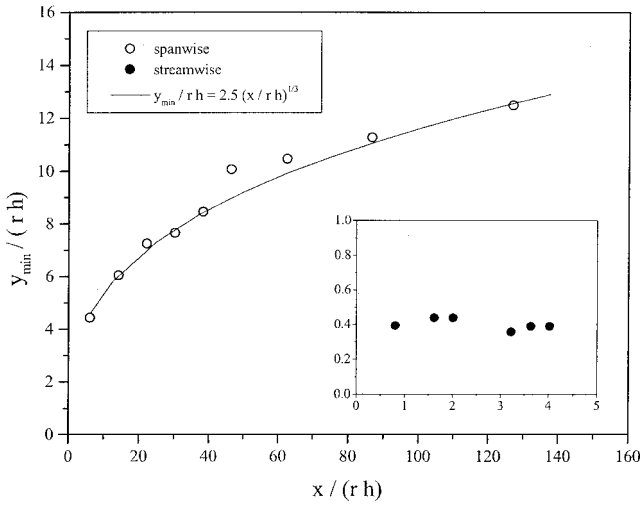

Fig. 16 Variation in the synthetic jet penetration depth with streamwise distance for the spanwise and streamwise (see inset) configuration; a constant x displacement has been substracted from the spanwise distribution to account for an apparent virtual origin located upstream of the geometric origin of the jet; the solid line is a one-third power law fit.

at $y/\delta_0 = 0.1$ at the centerline is filled in away from the centerline. This second observation is consistent with the motion of fluid in the boundary layer due to the vortex pair.

D. Cross-Stream Penetration

An important consideration for steady jets in a crossflow is the trajectory followed by the jet as it interacts with the crossflow. Both experimental measurements and the analyses of Broadwell and Breidenthal[16] and Hasselbrink and Mungal[17] reveal that for large velocity ratios and far from the jet origin the jet trajectory follows a power law in x. The power law has the form

$$y_{\min}/rh = A(x/rh)^B$$

where $y_{\min}$ is the point of minimum streamwise velocity within the wake region of the centerline velocity profiles, r is the velocity ratio, and h is the orifice height. This power law, with coefficients $A = 1.2$–2.6 and $B = 0.28$–0.34, describes well the trajectories of steady jets in a crossflow.

Figure 16 shows the downstream trajectories of the synthetic jet for the spanwise and streamwise configurations. By comparison with the power law, the synthetic jet in the spanwise configuration follows a trajectory quite similar to that of a steady jet in a crossflow. The leading coefficient A in the power law fit was increased from 1.5 to 2.5 to reflect the more rapid initial penetration of the synthetic jet, but remains consistent with the range of values of A reported in the literature. In addition, the formation of the jet from an oscillatory flow at the orifice gives rise to an apparent shift in the origin of the jet. The virtual origin of the synthetic jet lies downstream of the true synthetic jet position. To account for the virtual origin, the streamwise position of the jet in Fig. 16 has been shifted upstream by a constant amount. In considerable contrast, the jet trajectory for the streamwise configuration appears to be almost horizontal over the length of the measurement domain. Note that, for this configuration, h was replaced by w with the effect that x/rw is quite a bit smaller and closer to the jet origin. This result is important to the interpretation of the jet trajectory because the analysis by Broadwell and Breidenthal[16] applies only to large distances downstream of the jet origin, and this is clearly not the case for the streamwise configuration.

IV. Conclusions

The complete structure of the flow in the boundary layer downstream of the jet is difficult to understand fully from these measurements. Not unexpectedly, the interaction between the synthetic jet and the boundary layer is strongly influenced by the orientation of the synthetic jet orifice. In the spanwise configuration, the blockage of the flow is significant in the near field, and the flow downstream can be interpreted broadly as the wake of this obstruction, although there is evidence to suggest that this wake contains a distinct structure. In the streamwise configuration, the downstream flow appears to be influenced by secondary motions in the boundary layer. The mean velocity profiles suggest that high momentum fluid is swept toward the wall along the interaction centerline and away from the wall off center. Moreover, the velocity profiles are similar to those measured by Andreopoulos and Rodi[14] in a steady jet in crossflow.

A wall-jet character in the near-wall mean velocity profiles was observed in both configurations. However, in the spanwise configuration, this observation was a consequence of fluid moving into the low-pressure region in the lee of the jet, whereas in the streamwise configuration, this local extremum in the profile near the wall appears to be the result of secondary motions in the boundary layer.

The synthetic jets are initially high-aspect-ratio rectangular jets, but as they are turned downstream, they deform rapidly. In the spanwise configuration, the interaction scale appears to be as broad as the interaction for streamwise configuration, but does not penetrate to the same height in the boundary layer. For the spanwise configuration, the maximum penetration height is $0.8\delta_0$, whereas for the streamwise configuration, the interaction extends to the edge of the boundary layer. Clearly, as a jet in spanwise configuration presents a larger area to the oncoming flow, it is turned more rapidly downstream. In addition, the jet trajectory for the spanwise configuration was found to follow the power law scaling for a steady jet in a crossflow closely. The power law scaling is premised on the trajectory obtained by a counter-rotating vortex pair aligned in the streamwise direction. The good agreement with this scaling in the spanwise configuration suggests that the interaction contains a similar structure.

For the spanwise configuration, the observed trends in the integral parameters suggest that the synthetic jet is decoupled from the turbulent flow in the boundary layer, and, as its trajectory carries it beyond the boundary-layer edge, the boundary layer assumes characteristics consistent with its state before the interaction. In comparison with the spanwise configuration, the trends in the integral parameters suggest that the interaction in the streamwise configuration is still in the early stages of evolution. The displacement and momentum thickness both increase monotonically over the streamwise extent of the measurement domain, whereas the shape factor remains unchanged.

Finally, the Reynolds number in this set of experiments was quite low, $Re_\theta = 1.79 \times 10^3$. As the Reynolds number increases, we would expect the shape of the mean velocity profile to become fuller near the wall. We can speculate from the observations here that this change might affect the spanwise configuration to a greater extent as the interaction for that case takes place at lower levels in the boundary layer. For the streamwise configuration, because the jet rapidly penetrates into the upper region of the boundary layer, we would not expect a significant Reynolds number effect.

Acknowledgments

This work was funded through a grant from the Defense Advanced Research Projects Agency–Smart Aircraft and Marine Projects Demonstration program. This work was undertaken while the author was a Postdoctoral Fellow with Georgia Institute of Technology and The Boeing Company in St. Louis. The author is grateful to Ari Glezer for his comments during the preparation of the manuscript. The author would also like to acknowledge the assistance in this work provided by Dale Pitt and Mark Hopkins.

References

[1] Margason, R. J., "Fifty Years of Jets in Cross Flow," *Computational and Experimental Assessment of Jets in Cross Flow*, CP-534, AGARD, 1993, pp. 1–41.

[2] Johnston, J. P., and Nishi, M., "Vortex Generator Jets: Means for Flow Separation Control," *AIAA Journal*, Vol. 28, No. 6, 1990, pp. 989–994.

[3] Compton, D. A., and Johnston, J. P., "Streamwise Vortex Production by Pitched and Skewed Jets in a Turbulent Boundary Layer," *AIAA Journal*, Vol. 30, No. 3, 1992, pp. 640–647.

[4] Zhang, X., and Collins, M. W., "Measurements of a Longitudinal Vortex Generated by a Rectangular Jet in a Turbulent Boundary Layer," *Physics of Fluids*, Vol. 9, No. 6, 1997, pp. 1665–1673.

[5]Zhang, X., "Counter-Rotating Vortices Embedded in a Turbulent Boundary Layer with Inclined Jets," *AIAA Journal*, Vol. 37, No. 10, 1999, pp. 1277–1284.

[6]Bons, J., Sondergaard, R., and Rivir, R., "Control of Low-Pressure Turbine Separation Using Vortex Generator Jets," AIAA Paper 99-0367, June 1999.

[7]Rivir, R., "Passive and Active Control of Separation in Gas Turbines," AIAA Paper 2000-2235, June 2000.

[8]Amitay, M., Smith, B. L., and Glezer, A., "Aerodynamic Flow Control Using Synthetic Jet Technology," AIAA Paper 98-0208, Jan. 1998.

[9]Seifert, A., Darabi, A., and Wygnanski, I., "Delay of Airfoil Stall by Periodic Excitation," *Journal of Aircraft*, Vol. 33, No. 4, 1996, pp. 691–698.

[10]Magill, J., and McManus, K., "Exploring the Feasibility of Pulsed Jet Separation Control for Aircraft Configurations," *Journal of Aircraft*, Vol. 38, No. 1, 2001, pp. 48–56.

[11]Smith, D. R., Amitay, M., Kibens, V., Parekh, D., and Glezer, A., "Modification of Lifting Body Aerodynamics Using Synthetic Jet Actuators," AIAA Paper 98-0209, Jan. 1998.

[12]Amitay, M., Smith, D. R., Kibens, V., Parekh, D. E., and Glezer, A., "Aerodynamic Flow Control over an Unconventional Airfoil Using Synthetic Jet Actuators," *AIAA Journal*, Vol. 39, No. 3, 2001, pp. 361–370.

[13]Smith, B. L., and Glezer, A., "The Formation and Evolution of Synthetic Jets," *Physics of Fluids*, Vol. 10, No. 9, 1998, pp. 2281–2297.

[14]Andreopoulos, J., and Rodi, W., "Experimental Investigation of Jets in a Crossflow," *Journal of Fluid Mechanics*, Vol. 138, 1984, pp. 93–127.

[15]Crabb, D., Durao, D. F. G., and Whitelaw, J. H., "A Round Jet Normal to a Crossflow," *Journal of Fluids Engineering*, Vol. 103, No. 1, 1981, pp. 142–153.

[16]Broadwell, J. E., and Breidenthal, R. E., "Structure and Mixing of a Transverse Jet in Incompressible Flow," *Journal of Fluid Mechanics*, Vol. 148, 1984, pp. 405–412.

[17]Hasselbrink, E., and Mungal, M., "Transverse Jet and Jet Flames. Part 1. Scaling Laws for Strong Transverse Jets," *Journal of Fluid Mechanics*, Vol. 443, 2001, pp. 1–25.

J. P. Gore
Associate Editor